nature

https://doi.org/10.1038/s41586-023-06162-w

Accelerated Article Preview

Absence of near-ambient superconductivity in $LuH_{2\pm x}N_y$

Received: 16 March 2023

Accepted: 3 May 2023

Accelerated Article Preview

Cite this article as: Ming, X. et al. Absence of near-ambient superconductivity in $LuH_{2\pm x}N_y$. *Nature* https://doi.org/10.1038/s41586-023-06162-w (2023)

Xue Ming, Ying-Jie Zhang, Xiyu Zhu, Qing Li, Chengping He, Yuecong Liu, Tianheng Huang, Gan Liu, Bo Zheng, Huan Yang, Jian Sun, Xiaoxiang Xi & Hai-Hu Wen

Absence of near-ambient superconductivity in $LuH_{2\pm x}N_y$

Xue Ming[1,2], Ying-Jie Zhang[1,2], Xiyu Zhu[1*], Qing Li[1*], Chengping He[1], Yuecong Liu[1], Tianheng Huang[1], Gan Liu[1], Bo Zheng[1], Huan Yang[1], Jian Sun[1], Xiaoxiang Xi[1] & Hai-Hu Wen[1*]

[1] National Laboratory of Solid State Microstructures and Department of Physics, Collaborative Innovation Center of Advanced Microstructures, Nanjing University, Nanjing 210093, China

[2] These authors contributed equally to this work

Request for materials should be addressed to corresponding authors Hai-Hu Wen, hhwen@nju.edu.cn; Qing Li, liqing1118@nju.edu.cn; Xiyu Zhu, zhuxiyu@nju.edu.cn

Summary

Recently near-ambient superconductivity was claimed in nitrogen-doped lutetium hydride[1]. This stimulates a worldwide interest about exploring room temperature superconductivity under low pressures. By using a high pressure and high temperature synthesis technique, we have successfully obtained the nitrogen doped lutetium hydride ($LuH_{2\pm x}N_y$) with a dark-blue color and a structure with the space group of $Fm\bar{3}m$ evidenced by x-ray diffraction. This structure is the same as that reported in ref. 1, with a slight difference in lattice constant. The Raman spectroscopy also shows similar patterns between our samples and that in ref. 1. The energy dispersive X-ray spectroscopy (EDS) confirmed the existence of

nitrogen in the samples. At ambient pressure, we witness a metallic behavior from 350 down to 2 K. By applying pressures from 2.1 to 41 GPa, we observe a gradual color change from dark-blue, to violet, to pink-red. By measuring the resistance at pressures from 0.4 to 40.1 GPa, we have seen a progressively improved metallic behavior without showing superconductivity down to 2 K. Temperature dependence of magnetization under high pressures shows a very weak positive signal between 100 and 320 K, and the magnetization increases with magnetic field at 100 K, all these are not expected for superconductivity at 100 K. Thus, we conclude the absence of near-ambient superconductivity in this nitrogen-doped lutetium hydride under pressures below 40.1 GPa.

Main text

Metallic hydrogen and hydrogen-rich materials provide interesting platforms for searching room temperature superconductivity since it was proposed theoretically by Ashcroft[2]. However, experimentally it is difficult to achieve high temperature superconductivity (HTS) under low pressures[3, 4]. Then theorists proposed that the polyhydrides may have the potential to realize HTS due to the effect of internal chemical pressure[5]. Later, HTS was observed by experiments in H_3S with a transition temperature (T_c) above 200 K under a high pressure (~200 GPa) as predicted by the theories[6-8]. After that, more and more hydrogen-rich superconductors have been discovered, such as LaH_{10}, CaH_6, *etc.*[9-15]. However, according to the basic understanding on the theory of Bardeen-Cooper-Schrieffer (BCS), HTS would rely on

very strong electron-phonon coupling with a very high Debye temperature. According to the McMillan's formula, if we assume a Debye temperature of 500 K, the Coulomb screening constant $\mu^* = 0.13$, the requested electron-phonon coupling constant λ would be as large as 12.2 for $T_c = 100$ K. This huge λ cannot allow a stable lattice structure, thus this HTS can only be achieved in such systems when they are protected by extremely high pressures.

Recently, superconductivity at about 294 K in N-doped Lu hydride under only 1 GPa was reported[1], which is extremely interesting and important if the observation could be repeated. As reported by Dasenbrock-Gammon *et al.*[1], the dark-bluish ternary compound (with the formula $LuH_{3-\delta}N_{\varepsilon}$ used by them) can be tuned to a near-ambient superconductor by a relatively low pressure (1-2 GPa), accompanied with a color change from blue to pink and red. Actually, in previous experiments, superconductivity with much lower T_c was reported by other groups under high pressures in Lu hydrides[16,17]. Thus, comparing with above results of Lu hydrides, the discovery of near-ambient superconductivity in N-doped lutetium hydride is really striking. It generates great curiosity whether room temperature superconductivity really exists in this N-doped lutetium hydride under relatively low pressures.

Physical properties at ambient pressure

Figure 1**a** shows the X-ray diffraction (XRD) pattern and Rietveld refinement for the $LuH_{2\pm x}N_y$ sample. As we can see, the experimental data can be well fitted by the structure of LuH_2 with the space group of $Fm\bar{3}m$ and lattice parameter $a = 5.032(3)$ Å. It is known that the LuH_3 with a face-centered cubic structure is not stable at ambient

pressure, but a hexagonal structure with a space group of $P\bar{3}c1$ was reported[18,19]. As shown in Fig. 1**b**, the main reflections of XRD data in our sample SX1 and that downloaded from ref. 1 almost coincide, indicating that they have similar structure. The lattice constant of our sample SX1 is about a = 5.032(3) Å, which is a bit larger than a = 5.0289 Å reported in ref.1, but is very close to 5.033 Å determined previously[19,20] in LuH_2. For checking the lattice constants of our samples more carefully, we did a series of XRD measurements on different samples and found that the lattice constant ranges from 5.029(2) to 5.033(3) Å, see Extended Data Fig.1. Comparing with that in ref. 1, our samples show much less amount of impurities. Therefore, according to our XRD data, we obtained the compounds which have almost the same structure as that reported in ref. 1.

The energy dispersive X-ray spectroscopy (EDS) is used to analyze the element composition in the sample. The inset (left-hand side) in Fig. 1**c** displays a SEM image of $LuH_{2\pm x}N_y$ with randomly measured 10 spots marked by the black crosses. The compositions of nitrogen at these spots are given in the Extended Data Table I. The typical EDS of spot 1 is shown in the main panel of Fig. 1**c**, a weak peak from nitrogen can be identified. The right-hand side inset of Fig. 1**c** shows the spatial distribution of nitrogen, it looks wide-spreading in the whole area, but locally inhomogeneous. Since it is impossible to detect the hydrogen atoms by EDS, while XRD shows that the structure is quite consistent with LuH_2, we define the chemical formula of our samples as $LuH_{2\pm x}N_y$. Figure 1**d** displays the temperature dependence of resistivity (ρ-T) for three samples of $LuH_{2\pm x}N_y$ at ambient pressure. All samples show a metallic behavior

down to 2 K. The magnetization was measured for the sample at 10 Oe in the zero-field-cooling (ZFC) and field-cooling (FC) modes. The signal is positive and generally very small, see Extended Data Fig.2.

Raman spectroscopy

We also collected Raman spectra of our $LuH_{2\pm x}N_y$ samples at ambient pressure by using two different instruments both with 532 nm laser excitations. We name these instruments as Raman spectrometer #1 and #2 (see Methods). The Raman spectra measured on three of our samples at ambient pressure are displayed in Fig. 2**a**, the data from ref.1 is shown together for comparison (red curve). The Raman spectra of our samples (SR1-SR3) almost coincide with each other, indicating the uniform crystallinity. Moreover, the band positions of Raman spectra at around 150 cm^{-1}, 190 cm^{-1}, 250 cm^{-1}, and 1200 cm^{-1} (as shown by the dashed lines in Fig. 2**a**) in our samples are highly consistent with that reported by Dasenbrock-Gammon *et al.*[1]. The good consistency on Raman spectrum indicates that our samples are very similar to that reported in ref. 1. We also notice that the spectra collected by using Raman spectrometer #1 on samples SR1 and SR2 below 140 cm^{-1} deviate from that in ref. 1. In their work, the authors observed only one peak in the range from 100 to 140 cm^{-1}, but in our samples SR1 and SR2, there exist several tiny peaks. After taking a careful check on our Raman spectrometer #1, we find that these tiny peaks below 140 $cm^{-1}$are extrinsic and due to the instrument (see Extended Data Fig.3). To further prove that, we used Raman spectrometer #2 to measure on another sample (SR3), which is shown as the green curve in Fig. 2**a**. We can see that the Raman spectrum of sample SR3 is very

similar to that reported in ref. 1. Unfortunately, the Raman spectrometer #2 is not suitable for measurements involving a high pressure cell due to the limitation by its objective lens with a short working distance.

Figure 2**b** shows the Raman spectrum of the $LuH_{2\pm x}N_y$ sample (SR1) under various pressures up to 33.4 GPa. Because the Raman band of 1200 cm^{-1} overlaps with the characteristic band of diamond anvils under high pressures, and the one at around 190 cm^{-1} is rather weak, we only focus on the two bands at around 146 cm^{-1} and 250 cm^{-1}. Upon compression, these two Raman bands shift to higher wavenumbers, suggesting a sizeable change of interatomic interaction with pressure. We also conducted an independent control experiment up to 26.6 GPa for another $LuH_{2\pm x}N_y$ sample (SR2), see Extended Data Fig.4. Both sets of data show good agreement with each other.

We then extracted the wavenumbers of these two bands in the Raman spectra under different pressures, and summarized the pressure-dependent band positions in Fig. 2**c**. It is found that the frequencies of Raman bands at around 146 cm^{-1} and 250 cm^{-1} show a continuous increase with increasing pressure. With careful analysis of the data, we found that the slope of the two curves changes obviously around 10 GPa, as shown by the diversion from the red solid lines. Then there is another slight change at around 20 GPa. As we know, in ref. 1, the abnormal changes of Raman band shift under pressure were correlated with three distinct phases. The anomalous Raman band shifts of our samples under high pressures seem to be consistent with that reported by Dasenbrock-Gammon *et al.*[1], except for different thresholds for pressure at which the slope-change occurs. We want to emphasize that these slope-changes are not necessarily associated

with three distinct phases, rather the fact that all phonons are unharmonic, and they tend to react to compression more steeply for a low pressure, and less steeply for a high pressure.

Resistance and colors at high pressures

Figure 3**a**, **b** show the temperature dependence of resistance from 10 to 350 K under various pressures. The resistance at room temperature progressively decreases with the increase of pressure up to 6.3 GPa. The temperature dependent resistance *R*(T) curve shows a universal hump structure around 300 K, and such feature becomes weaker for higher pressures. This hump reflects a metal to semiconductor transition, which may share the same origin as that observed in hydrides of many other rare-earth elements[21, 22]. To check whether the decrease in resistance around room temperature is related to a possible superconducting transition, we have also measured *R*(T) curves of $LuH_{2\pm x}N_y$ at various magnetic fields under a pressure of 1.6 GPa. As we can see from Fig. 3**c**, the resistance under magnetic fields exhibits a non-systematic evolution and does not show any drifting to lower temperatures as expected for a superconductor when a magnetic field is applied.

One of the most surprising phenomena reported in ref. 1 is the color change from dark-blue to pink, and red with increasing pressure. And the near-ambient superconductivity was claimed in the state with the pink color. We also tried to see this color change in our samples with pressures up to 5.2 GPa (Extended Data Fig. 5), but the dark-blue color was maintained. The pressure threshold for the color change seems to be sample dependent, in the nitrogen-free[23, 24] or nitrogen doped samples[25, 26]. Thus

we tried another run of optical measurements with pressures up to 41 GPa, now the color change can be clearly visualized. As shown in Fig. 4**a**, the color gradually changes from dark-blue to violet, and then to pink-red, the crossover from dark-blue to pink-red occurs in the region from about 11 GPa to about 21 GPa, then the color stays as pink-red. A general chart for the correlation between the color change and pressure for different samples is shown in Extended Data Fig. 6. We found that the pressure region of the color change was pretty consistent with the Raman band-shift anomaly shown in Fig. 2**c**. Although there is a recent literature on photochromism of $LnH_{2+x}O_y$ (*Ln* = lanthanide element)[27], which suggests that this effect may lead to the pink color, however, we would argue that this is not the reason for the pink-red color in our samples since it gradually emerges with increase of pressure, and the pink-red color appears almost in the whole sample under a high pressure. This color change may be explained by the shift of the plasma edge of a metal[24] when it has a low charge carrier density; the latter can be easily tuned by pressure in systems containing shallow bands. Given the color change from dark-blue to pink-red, it is curious to know whether the claimed superconductivity in ref. 1 can be found in this high pressure range, especially with a pink-red color.

We then carried out a new run of measurements on resistivity from 0.4 to 40.1 GPa, the data are shown in Fig. 4**b**. One can clearly see that the general behavior is metallic for the states under all pressures. We also measured the temperature dependent resistance under 15.8 GPa at three different magnetic fields (0, 50, 90 kOe), and found a negative magnetoresistance, which contradicts to the expectation for a

superconducting state, see Extended Data Fig. 7. Thus we can safely conclude that no superconductivity is observed under pressures below 40.1 GPa and above 2 K from resistance measurements.

Magnetic moments under high pressures

To check whether there is a diamagnetic signal due to the Meissner effect of the possible superconductivity in our as-grown samples, we measured temperature dependent DC magnetization M(T) curves of $LuH_{2\pm x}N_y$ with pressures of 1 GPa and 2.1 GPa. The sample volume for the high pressure measurement is about 0.037 mm^3. The M(T) curves at 60 Oe (the same field used in ref.1) under different pressures are shown in Fig. 5**a**, **b**. The magnetic moment increases with decreasing temperature and do not show a sudden drop behavior. Furthermore, due to the background signal of the magnetization measurement device (Honest Machinery Designer, abbreviated as HMD), the values of the total magnetic moment are negative in the whole measured temperature region. In order to get the magnetization signal purely from the sample, we also measured the background signal of the HMD cell at 60 Oe. The data of background signal are presented in Extended Data Fig.8. The net magnetic moments after removing the related background are shown in the insets of Fig. 5**a** and 5**b**. One can see that the net signal of magnetic moment is positive and very weak with a roughly flat feature in the temperature region from 100 to 320 K. The inset of Fig. 5**c** displays the isothermal magnetization M(H) curves for $LuH_{2\pm x}N_y$ at 100 K under pressures of 1 GPa (open squares) and 2.1 GPa (open circles). The M(H) curve shows a roughly linear behavior with a negative slope from 0 to 6,000 Oe, which is due to the background. To prove

that, we have measured one *M*(H) curve at 320 K under 2.1 GPa (up triangle), and one curve at 100 K for the empty HMD cell (solid square). In the main panel of Fig. 5**c**, we show the net *M*(H) curves after subtracting related backgrounds. It is clear that all net *M*(H) curves exhibit a roughly linear behavior with a positive correlation. This corresponds to a possible paramagnetic behavior. We also conducted a new run for magnetization measurement on another $LuH_{2\pm x}N_y$ sample up to 4.5 GPa, see Extended Data Fig.9. The same HMD cell was successfully used to detect a clear superconducting transition in Bi samples before[28]. To prove that this setup is equally sensitive to detect a superconducting phase in the high temperature region, we carried out magnetization measurements on a superconducting sample $(Cu,C)Ba_2Ca_3Cu_4O_{12}$ ($T_c \approx 112$ K)[29, 30], the data are shown in Fig. 5**d**. One can see that the signal is negative and huge compared with $LuH_{2\pm x}N_y$. Our magnetization measurements with the data of either temperature dependence or the isothermal magnetization curves all show that there is no any trace of near-ambient superconductivity in $LuH_{2\pm x}N_y$. The absence of near-ambient superconductivity in nitrogen doped lutetium hydrides is supported by recent theoretical calculations[31-34].

In summary, we have successfully synthesized the N-doped lutetium hydrides $LuH_{2\pm x}N_y$ with a dark-blue color. Although our synthesis method is different, the XRD and Raman spectroscopy confirmed that our samples have a similar structure as the main phase reported in ref. 1 with a slight difference of lattice constant. Meanwhile, the existence of nitrogen in our samples is also confirmed by EDS analysis. We also visualized a color change from dark-blue to violet, and pink-red upon applying high

pressures, although the threshold pressures for the color change are higher than that in ref. 1. Our resistivity measurements show the absence of superconductivity in $LuH_{2\pm x}N_y$ under pressures up to 40.1 GPa with all different colors down to 2 K. The magnetization measurements further prove that no superconductivity exists in $LuH_{2\pm x}N_y$ above 100 K under near-ambient pressures.

References

1. Dasenbrock-Gammon, N. et al. Evidence of near-ambient superconductivity in a N-doped lutetium hydride. *Nature* **615**, 244-250 (2023).
2. Ashcroft, N. W. Metallic hydrogen: A high-temperature superconductor? *Phys. Rev. Lett.* **21**, 1748 (1968).
3. Dias, R. P. & Silvera, I. F. Observation of the Wigner-Huntington transition to metallic hydrogen. *Science* **355**, 715-718 (2017).
4. Mao, H. K., Chen, X. J., Ding, Y., Li, B. & Wang, L. Solids, liquids, and gases under high pressure. *Rev. Mod. Phys.* **90**, 015007 (2018).
5. Ashcroft, N. W. Hydrogen dominant metallic alloys: high temperature superconductors? *Phys. Rev. Lett.* **92**, 187002 (2004).
6. Li, Y., Hao, J., Liu, H., Li, Y. & Ma, Y. The metallization and superconductivity of dense hydrogen sulfide. *J. Chem. Phys.* **140**, 174712 (2014).
7. Duan, D. et al. Pressure-induced metallization of dense $(H_2S)_2H_2$ with high-T_c superconductivity. *Sci. Rep.* **4**, 6968 (2014).
8. Drozdov, A. P., Eremets, M. I., Troyan, I. A., Ksenofontov, V. & Shylin, S. I.

Conventional superconductivity at 203 kelvin at high pressures in the sulfur hydride system. *Nature* **525**, 73-76 (2015).

9. Geballe, Z. M. et al. Synthesis and stability of lanthanum superhydrides. *Angew. Chem. Int. Ed.* **57**, 688-692 (2018).
10. Drozdov, A. P. et al. Superconductivity at 250 K in lanthanum hydride under high pressures. *Nature* **569**, 528-531 (2019).
11. Li, Z. et al. Superconductivity above 200 K discovered in superhydrides of calcium. *Nat. Commun.* **13**, 2863 (2022).
12. Ma, L. et al. High-temperature superconducting phase in clathrate calcium hydride CaH_6 up to 215 K at a pressure of 172 GPa. *Phys. Rev. Lett.* **129**, 269901 (2022).
13. Kong, P. et al. Superconductivity up to 243 K in the yttrium-hydrogen system under high pressure. *Nat. Commun.* **12**, 5075 (2021).
14. Snider, E. et al. Synthesis of yttrium superhydride superconductor with a transition temperature up to 262 K by catalytic hydrogenation at high pressures. *Phys. Rev. Lett.* **126**, 117003 (2021).
15. Chen, W. et al. High-temperature superconducting phases in cerium superhydride with a T_c up to 115 K below a pressure of 1 megabar. *Phys. Rev. Lett.* **127**, 117001 (2021).
16. Shao, M. et al. Superconducting ScH_3 and LuH_3 at megabar pressures. *Inorg. Chem.* **60**, 15330-15335 (2021).
17. Li, Z. et al. Superconductivity above 70 K observed in lutetium polyhydrides. *Sci. China. Phys. Mech. Astron.* **66**, 267411 (2023).

18. Dierkes T., Plewa, J. & Jüstel, T. From metals to nitrides - Syntheses and reaction details of binary rare earth systems. *J. Alloy Compd.* **693**, 291-302 (2017).
19. Pebler, A. & Wallace, W. E. Crystal structures of some lanthanide hydrides. J. Phys. Chem. **66**, 148-151 (1962).
20. Bonnet, J. E. & Daou, J. N. Rare-earth dihydride compounds: Lattice thermal expansion and investigation of the thermal dissociation. J. Appl. Phys. **48**, 964, (1977).
21. Huiberts, J. N., Griessen, R., Wijngaarden, R. J., Kremers, M. & Haesendonck, C. V. Logarithmic divergence of the electrical resistivity in the metal hydride $YH_{3-\delta}$. *Phys. Rev. Lett.* **79**, 3724 (1997).
22. Vajda, P. *Handbook on the Physics and Chemistry of Rare Earths* 251-255 (Elsevier, 1995).
23. Shan, P. et al. Pressure-induced color change in the lutetium dihydride LuH_2. *Chin. Phys. Lett.* **40**, 046101 (2023).
24. Zhao, X. et al. Pressure tuning of optical reflectivity in LuH2. arXiv: 2303.16745 (2023).
25. Zhang, Y. J. et al. Pressure induced color change and evolution of metallic behavior in nitrogen-doped lutetium hydride. arXiv: 2303.17453 (2023).
26. Xing, X. et al. Observation of non-superconducting phase changes in $LuH_{2\pm x}N_y$. arXiv: 2303.17587 (2023).
27. Nafezarefi, F., Schreuders, H., Dam, B. & Cornelius S. Photochromism of rare-earth metal-oxy-hydrides. *Appl. Phys. Lett.* **111**, 103903 (2017).

28. Li, Y., Wang, E., Zhu, X. & Wen, H. H. Pressure-induced superconductivity in Bi single crystals. *Phys. Rev. B* **95**, 024510 (2017).
29. Zhang, Y. et al. Unprecedented high irreversibility line in nontoxic cuprate superconductor (Cu,C)$Ba_2Ca_3Cu_4O_{11+\delta}$. *Sci. Adv.* **4**, eaau0192 (2018).
30. He, C. et al. Characterization of the (Cu,C)$Ba_2Ca_3Cu_4O_{11+\delta}$ single crystals grown under high pressure. *Supercond. Sci. Tech.* **35**, 025004 (2022).
31. Huo, Z. et al. First-principles study on the superconductivity of N-doped fcc-LuH_3. arXiv: 2303.17587 (2023).
32. Kim, S.-W. et al. Microscopic theory of colour in lutetium hydride. arXiv: 2304.07326 (2023).
33. Ferreira, P. P. et al. Search for ambient superconductivity in the Lu–N–H system. arXiv: 2304.04447 (2023).
34. Lu, T., Meng, S. & Liu, Miao. Electron-phonon interactions in LuH_2, LuH_3, and LuN. arXiv: 2304.06726 (2023).

Methods

Sample preparation and characterization. We synthesized polycrystalline samples of $LuH_{2\pm x}N_y$ using a piston-cylinder type high pressure apparatus (LP 1000-540/50, Max Voggenreiter). The NH_4Cl and excessive CaH_2 were used as the source of nitrogen and hydrogen, according to the chemical reaction equation written as $2NH_4Cl + CaH_2 \rightarrow CaCl_2 + 2NH_3 + H_2$. The NH_4Cl (Alfa Aesar 99.99%) was mixed well with CaH_2 (Alfa Aesar 98%) in a molar ratio of 2:8 and pressed into a tablet. Then, the tablet made by

Lu pieces (purity 99%, Grirem Advanced Materials Co. Ltd.) with silver color were separated from the tablet of $NH_4Cl+CaH_2$ by a BN pellet and sealed into a gold capsule. The Lu pellet in each sintering weighs about 100 mg. Then the gold capsule was placed in a BN capsule and heated up to 300-350°C and held for 10 hours under 2 GPa. Finally, we find that the Lu tablet turns into a new form composed by two well-separated different regions with dark-blue and silver colors, respectively; the dark-blue region corresponds to the $LuH_{2\pm x}N_y$ phase.

The X-ray diffraction (XRD) measurements were performed on a Bruker *D8* Advanced diffractometer with the CuK_α radiation. The Rietveld refinements were done by using the software[35] of *TOPAS4.2*. The scanning electron microscope (SEM) photograph and the energy dispersive X-ray microanalysis spectrum were obtained by Phenom ProX (Phenom) at an accelerating voltage of 15 kV. Unpolarized Raman-scattering experiments were performed using two instruments at room temperature both with a 532 nm laser excitation line, one is a Raman spectroscopy system (LabRAM HR Evolution Horiba Jobin Yvon), the other one is a home built confocal microscopy setup in the back-scattering geometry in which the scattered light was directed through Bragg notch filters. For clarity, we name the first Raman system as Raman spectrometer #1, and the second Raman system as Raman spectrometer #2. Prior to the measurements, both systems were calibrated for wavenumbers by following the instrument instructions. To get valid data in the low wavenumber region (below 140 cm^{-1}), we used Raman spectrometer #2 for the Raman scattering measurement on a new sample (SR3) placed in vacuum. By the way, before the measurement on the sample SR3, we checked the

Raman spectrometer #2 without a sample, and find a smooth background without any band like features in the low wavenumber region. For the measurements using Raman spectrometer #1 and #2, the laser power was 7.5 and 4 mW, the collection time was 60 and 120 seconds, respectively, and all spectra were measured two times to check reproducibility. For high pressure Raman spectra measurements, two runs of experiments were performed on Raman spectrometer #1 by using a diamond anvil cell (DAC) with T301 steel or rhenium as gasket and methanol/ethanol/water as pressure medium.

Physical property measurements at ambient and high pressures. Temperature dependent resistivity/resistance measurements under ambient and high pressure were carried out with a physical property measurement system (PPMS-9T, Quantum Design). The high pressure was generated by a DAC made of BeCu alloy with two opposing anvils. A four-probe van der Pauw method with platinum foil as electrodes was applied for resistance measurements. The DC magnetization measurements were performed with a SQUID-VSM-7T (Quantum Design). The DC magnetic moment measurements at high pressures were accomplished by using the DAC (attachment to a PPMS) designed by the Honest Machinery Designer's office (HMD). The sample is loaded in a hole in the middle of the gasket made of BeCu which needs pre-pressurization before high-pressure measurements. The gasket is made by BeCu. The anvils with beveled culet size of 400 μm and 600 μm were used to generate high pressures. NaCl and Daphne 7373 were used as the pressure transmitting medium during the resistive and

magnetic susceptibility measurements, respectively. For optical measurements, we used KBr as the pressure transmitting medium. The pressure was measured at room temperature using the ruby fluorescence method[36].

Data availability statement

All data needed to evaluate the conclusions in the paper are present in the paper. Source data are provided with this paper.

35. Cheary, R. W. & Coelho, A. A. fundamental parameters approach to X-ray line-profile fitting. *J. Appl. Cryst.* **25**, 109-121 (1992).
36. Mao, H. K., Xu, J. & Bell, P. M. Calibration of the ruby pressure gauge to 800 kbar under quasi-hydrostatic conditions. *J. Geophys. Res.* **91**, 4673-4676 (1986).

Acknowledgements

This work was supported by the National Key R&D Program of China (No. 2022YFA1403201), National Natural Science Foundation of China (Nos. 12061131001, 12204231, 52072170, and 11927809), and Strategic Priority Research Program (B) of Chinese Academy of Sciences (No. XDB25000000).

Author contributions

The sample growth and SEM/EDS analysis were made by X.M., X.Y.Z., C.P.H., B.Z. and H.H.W. The XRD data were collected by Y.C.L. and X.M. The resistivity and

magnetization were measured by Q.L. and Y.J.Z. The photos were taken by H.Y. The Raman spectra were collected and analyzed by Q.L., T.H.H., G. L., X.X. and J.S. All authors joined the analysis and agreed to publish the data. The manuscript was written by Q.L., X.Y.Z. and H.H.W. H.H.W. conceived and supervised the whole research.

Author statement about reproducibility and control experiments

We have conducted multiple kinds of experiments on more than 30 samples: 7 specimens measured for resistivity at ambient pressure; 5 specimens for resistivity under high pressures; 2 specimens for magnetization measurements at ambient pressure; 3 specimens for magnetization measurements under high pressures; 6 specimens for XRD measurements; 3 runs (specimens) for the Raman spectroscopy measurements; 5 runs (specimens) for optical image measurements; 8 specimens for SEM/EDS measurements.

Competing interests

The authors declare that they have no competing interests.

Main Figure Legends

Fig. 1 | Structure, composition and transport measurements for $LuH_{2\pm x}N_y$. a, Powder X-ray diffraction patterns of the $LuH_{2\pm x}N_y$ and Rietveld fitting curves (red lines) to the data. The tiny reflection at 32.2° can be indexed to the phase of Lu_2O_3. The inset shows the picture of $LuH_{2\pm x}N_y$ samples which exhibit a dark-blue color. **b,** The comparison of XRD patterns with normalization between our sample SX1 and that

399 downloaded from ref. 1. The inset shows an enlarged view with 2θ from 29° to 37° for
400 two of our samples (SX1 and SX5) and that from ref. 1. The main reflections of our
401 samples look sharper than that in ref. 1. **c,** SEM images and typical EDS of spot 1. Inset
402 (left-hand side) shows the image with ten spots measured by point-wise measurement
403 of EDS; the inset on the right-hand side shows the mapping image for nitrogen elements.
404 It is clear that the nitrogen distribution is not uniform in the sample, and it remains to
405 be resolved at which positions these nitrogen atoms locate in the lattice. **d,** Temperature
406 dependence of resistivity for three $LuH_{2\pm x}N_y$ samples under ambient pressure. Inset
407 shows the image of the measured sample (S1) with electrodes attached at ambient
408 pressure. The error bar for determining resistivity is about ±10%. The ρ-T curves are
409 roughly linear from 60 to 300 K and exhibit a power-law temperature dependence at
410 lower temperatures (2-60 K). The red solid lines represent the fitting curves using the
411 formula $\rho = \rho_0 + AT^n$ from 2 to 60 K, with ρ_0 the residual resistivity, n and A are the
412 fitting parameters. The fitting yields n = 2.89, 2.71 for S2 and S3, respectively.
413
414 **Fig. 2 | Raman spectra of $LuH_{2\pm x}N_y$. a,** Typical Raman spectra collected at ambient
415 pressure for three samples (black, blue and green curves), and the data of N-doped Lu
416 hydride from ref. 1 (red curve) for comparison. The samples are labeled as SR1, SR2
417 and SR3, respectively. The tiny peaks of SR1 and SR2 below 140 cm^{-1} are shown to be
418 originated from the background signal of the Raman spectrometer #1 (See Extended
419 Fig.3). The band positions in the spectrum below 300 cm^{-1} have slightly smaller
420 wavenumbers compared with that in ref. 1, indicating that the lattice constant of our

sample is slightly larger. The results are also consistent with the lattice parameters obtained from X-ray diffraction. Such a slight variation may be attributed to the different hydrogen/nitrogen concentrations in different samples. **b,** Raman spectra were collected under high pressures by using Raman spectrometer #1 with methanol/ethanol as the pressure medium. **c,** The evolution of band positions of Raman spectra under pressures, the two curves correspond to the bands as indicated in (**b**) by red arrows. The red lines are guides for eyes to show the change of slopes.

Fig. 3 | Temperature-dependent resistance for $LuH_{2\pm x}N_y$ at different pressures up to 6.3 GPa. a, Temperature dependence of the electrical resistance of $LuH_{2\pm x}N_y$ from 10 to 350 K with pressures up to 6.3 GPa (DAC filled with polycrystalline pieces). The weak upturn of R(T) curve in low temperature region may be induced by the hopping of electrons through a large inter-grain spacing or grain boundaries when the grains are compacted loosely in the DAC space. This explanation can get a support from the weakening and absence of this low temperature upturn when the pressure becomes higher. **b,** Temperature dependence of the electrical resistance of $LuH_{2\pm x}N_y$ up to 2.7 GPa for another run with the DAC filled with powder of the sample. Now we can see that the low-temperature upturn disappears. **c,** Temperature dependence of the electrical resistance of $LuH_{2\pm x}N_y$ measured at different magnetic fields up to 90 kOe at 1.6 GPa (DAC filled with polycrystalline pieces).

Fig. 4 | Pressure induced color change and evolution of temperature-dependent

resistance for $LuH_{2\pm x}N_y$ at different pressures. a, The optical microscope images of $LuH_{2\pm x}N_y$ at different pressures up to 41 GPa. A color change from dark-blue to violet and pink-red is observed. **b,** Temperature dependence of the electrical resistance of $LuH_{2\pm x}N_y$ from 2 to 350 K with pressures up to 40.1 GPa. In most *R*(T) curves, we can see a metallic behavior from an intermediate temperature all the way down to 2 K, either in the dark-blue or the pink-red states. The *R*(T) curves at low pressures, such as at 0.4 and 1.1 GPa show again the weak upturn in low temperature region, which gradually becomes invisible when the pressure is increased. And there is a resistivity hump in the region around 300 K in the low pressure region.

Fig. 5 | Magnetic properties for $LuH_{2\pm x}N_y$ at different pressures. a, b, Temperature dependence of magnetic moment for $LuH_{2\pm x}N_y$ under pressures of 1 GPa and 2.1 GPa, respectively. Shown in the main panels are raw data. The insets show the corresponding magnetic moments measured in ZFC and FC modes with the background subtracted. **c,** *M(H)* curves with different background signal removed. The inset shows the raw data of *M(H)* curves at 100 K under pressures of 1.0 GPa (open square) and 2.1 GPa (circle), and one curve at 320 K under 2.1 GPa (up triangle), respectively. The *M*(H) curve measured at 100 K for the empty HMD cell is also shown here (solid square). **d,** Temperature dependence of ZFC-FC magnetizations measured on a superconducting sample $(Cu,C)Ba_2Ca_3Cu_4O_{11+\delta}$ (T_c = 112 K) with the same measured volume as that for $LuH_{2\pm x}N_y$ shown in (**a**) and (**b**), and the same HMD setup was used under the same magnetic field (60 Oe). If the phase $LuH_{2\pm x}N_y$ were superconductive, one should

observe a diamagnetic signal in the same scale at the same field (60 Oe).

Extended Data Table I | The atomic concentration of nitrogen by EDS analysis at 10 spots of the sample. The average value of nitrogen in atomic ratio over these 10 spots is about 1.2%.

Extended Data Fig. 1 | XRD and Rietveld refinement on other four samples. **a-d,** Powder X-ray diffraction patterns of four samples (SX2-SX5) and Rietveld fitting curves (red lines) to the data. The inset in (**d**) presents the Rietveld fitting results (lattice parameters and molar concentration of $LuH_{2\pm x}N_y$) of five samples (SX1-SX5). The slight difference of the lattice constants may be attributed to the different hydrogen/nitrogen concentrations or the crystallinity in different samples. The Rietveld fitting to these results shows a high purity with the main phase in a molar ratio of about 95%, and are highly consistent with each other.

Extended Data Fig. 2 | Temperature dependence of the magnetic susceptibility for $LuH_{2\pm x}N_y$ at ambient pressure. a, Temperature dependence of magnetic moment for $LuH_{2\pm x}N_y$ (upper part) along with background signal (lower part) measured in an applied field of 10 Oe using both the ZFC and FC modes. **b**, The corresponding magnetic susceptibility $4\pi\chi$ with the background subtracted, for a superconductor we should expect $4\pi\chi$ = -1. In calculating the magnetic susceptibility, we have used a density of 9.22 g/cm^2 quoted for compound LuH_2. The measurements were carried out by using the SQUID-VSM with a vibrating amplitude of 5 mm and frequency of 13.01 Hz.

Extended Data Fig. 3 | Raman spectra collected on Raman spectrometer #1. The black curve (upper one) shows the raw data measured on the $LuH_{2\pm x}N_y$ sample (SR1) using the Raman spectrometer #1, while the orange curve (bottom one) shows the background signal of the instrument without the sample nor the DAC. It is clear that the bands around 106 cm^{-1}, 115 cm^{-1}, 122 cm^{-1}, 129 cm^{-1} and 138 cm^{-1} are originated from the instrument itself.

Extended Data Fig. 4 | Raman spectra of another $LuH_{2\pm x}N_y$ sample (SR2) under different pressures. In this measurement, a rhenium gasket was used. The Raman bands around 146 cm^{-1} and 250 cm^{-1} show continuous increase with increasing pressure. Due to a sizeable Raman signal from the instrument under low wavenumbers, we show only the data above 140 cm^{-1}.

Extended Data Fig. 5 | The optical microscope images of $LuH_{2\pm x}N_y$ at different pressures up to 5.2 GPa. In this run, the sample was directly filled in the DAC chamber without any pressure medium.

Extended Data Fig. 6 | A sketch for pressure dependence of the color change for different samples. The data are collected from Fig. 4 **a** and ref 1, 23, 24, 25, 26.

Extended Data Fig. 7 | Temperature dependence of electrical resistance for $LuH_{2\pm x}N_y$. The measurements were conducted under a pressure of 15.8 GPa with various magnetic fields up to 90 kOe. The hump structure around 250-300 K is gradually suppressed by external fields and a negative magnetoresistance is observed. No superconducting signal was detected down to 2 K.

Extended Data Fig. 8 | Temperature dependence of magnetic moment for the empty HMD cell. The applied magnetic field was H = 60 Oe. The ZFC and FC M(T) curves are used as the background signals to obtain the magnetic moment purely from the sample in the DC magnetization measurements.

Extended Data Fig. 9 | Temperature dependence of magnetic moment for $LuH_{2\pm x}N_y$. All curves were measured in an applied field of 60 Oe using both the ZFC and FC modes in run 2 at pressures of **(a)** 1.5 GPa and **(b)** 4.5 GPa. The raw data are shown in the main panels. The insets show the corresponding magnetization with the background signal removed. The magnetic susceptibility for $LuH_{2\pm x}N_y$ is positive in the whole temperature region, and no diamagnetic signal was detected, which is contrary

526 to the existence of superconductivity.

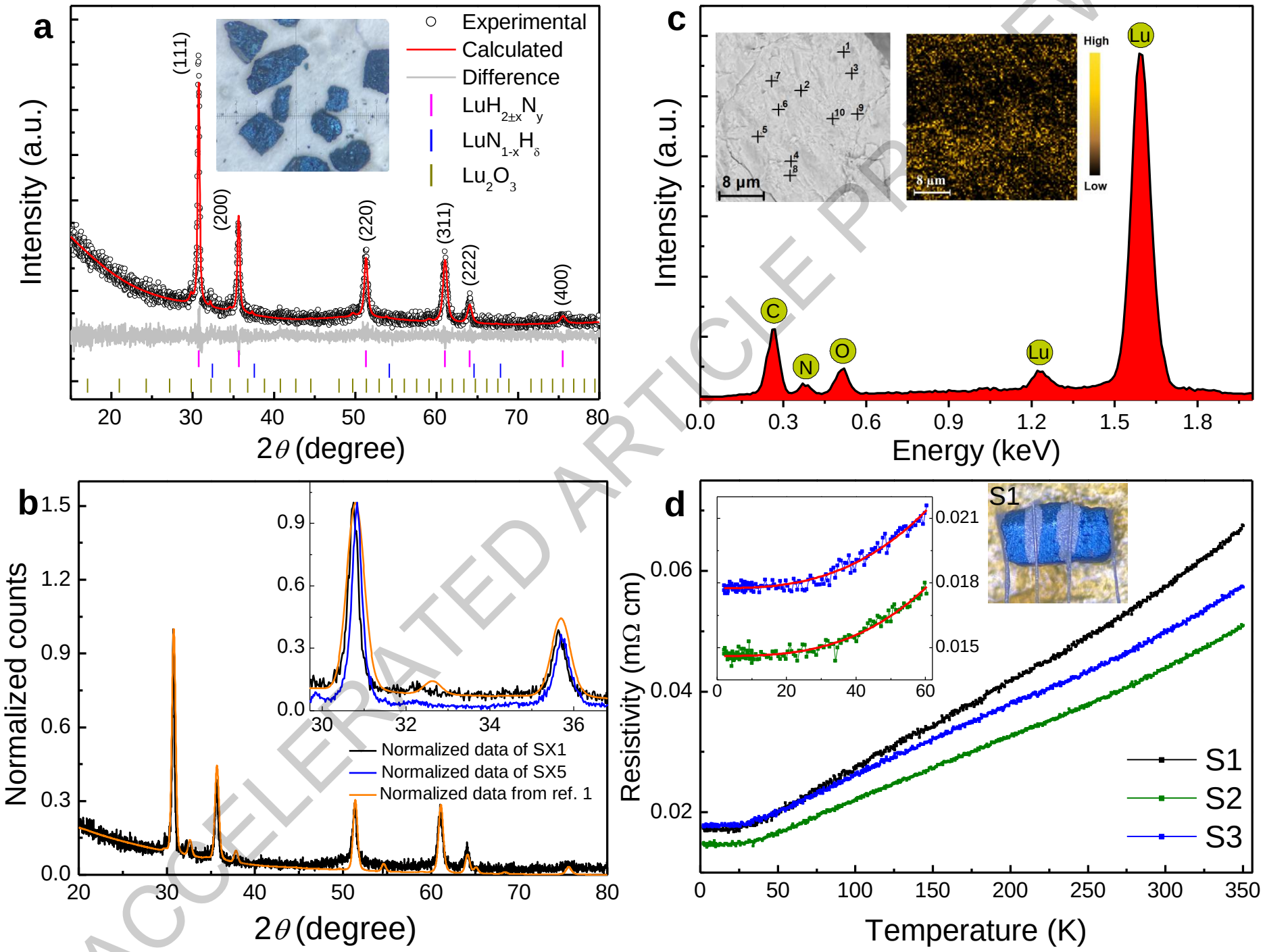

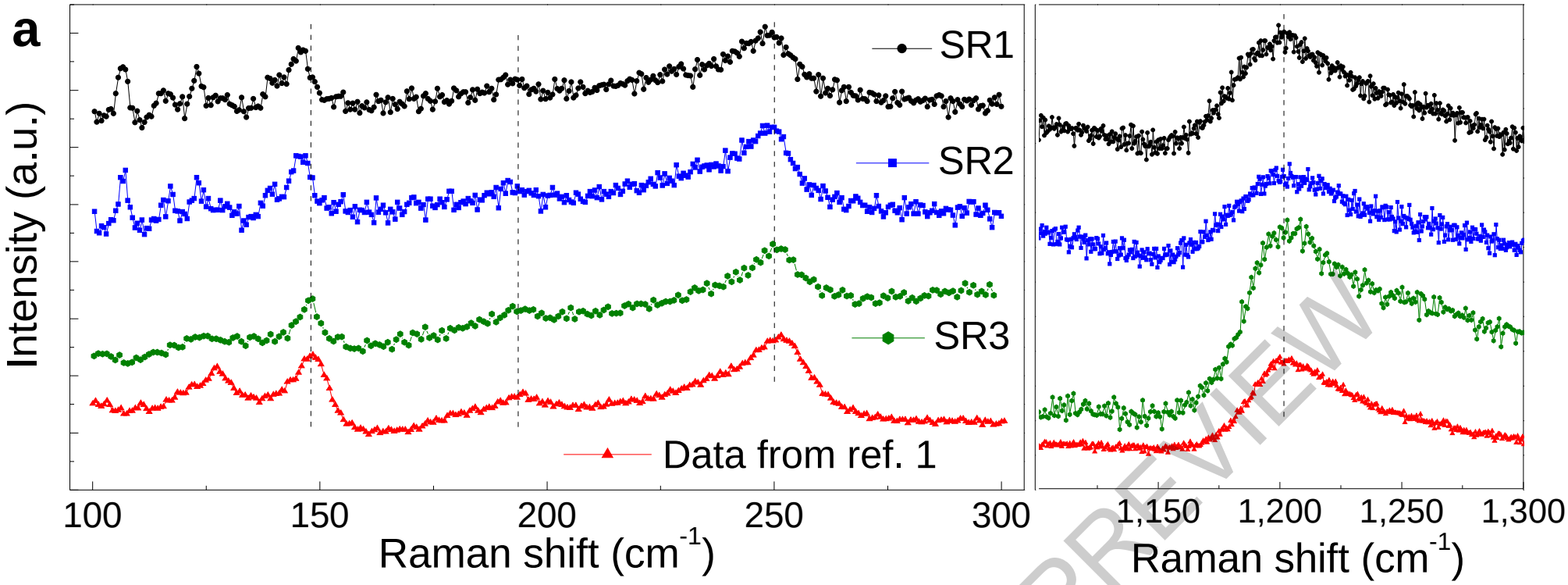

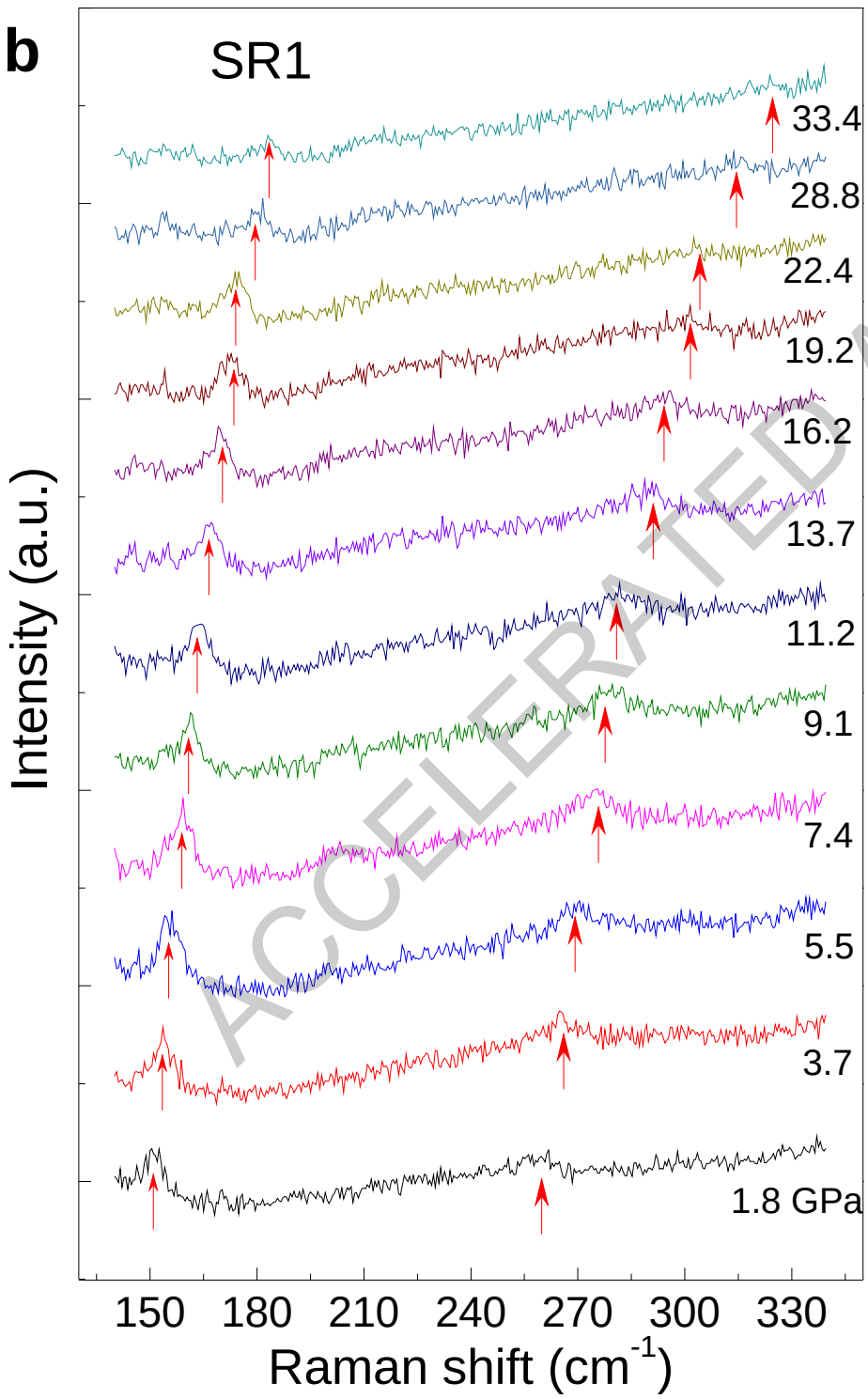

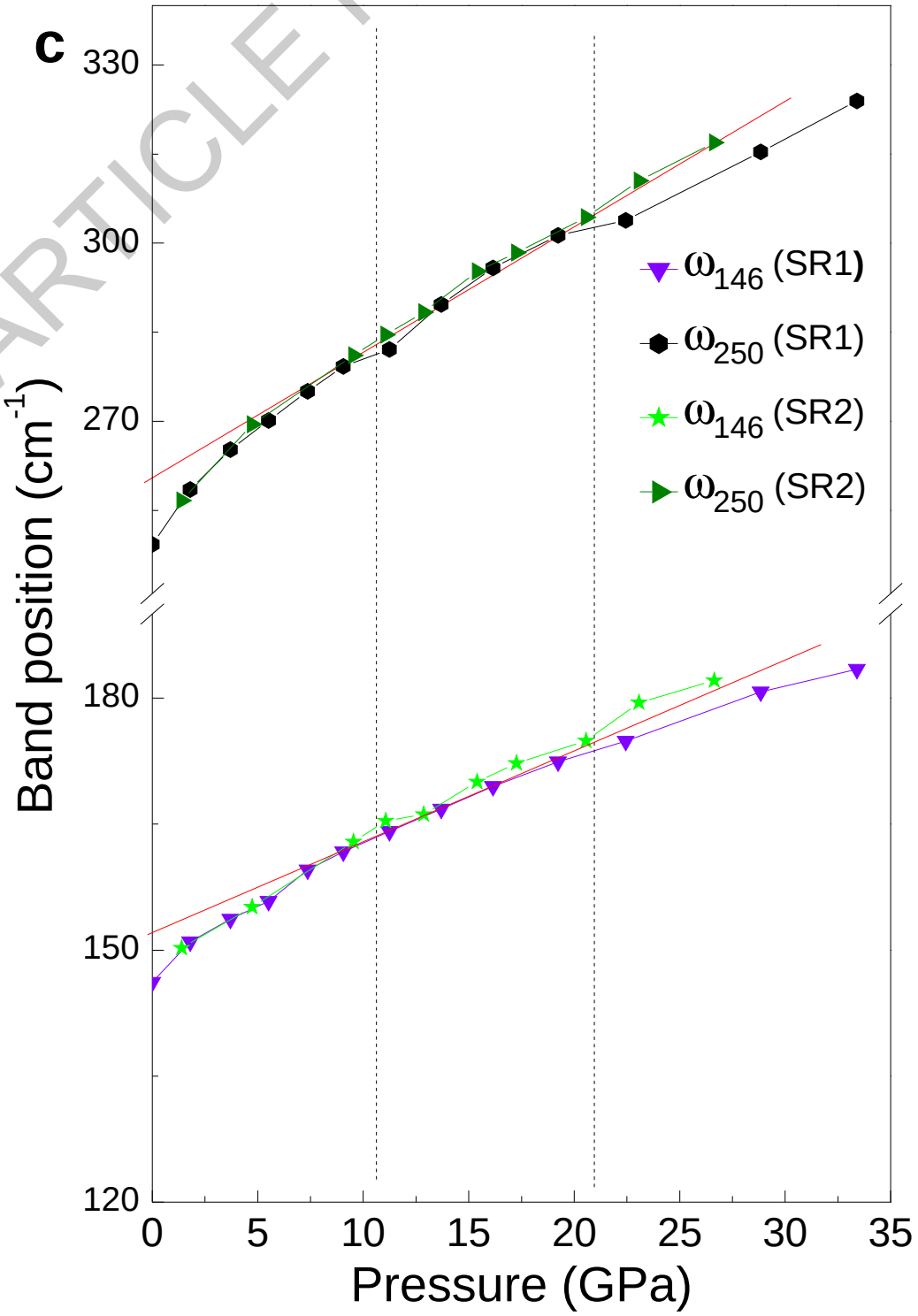

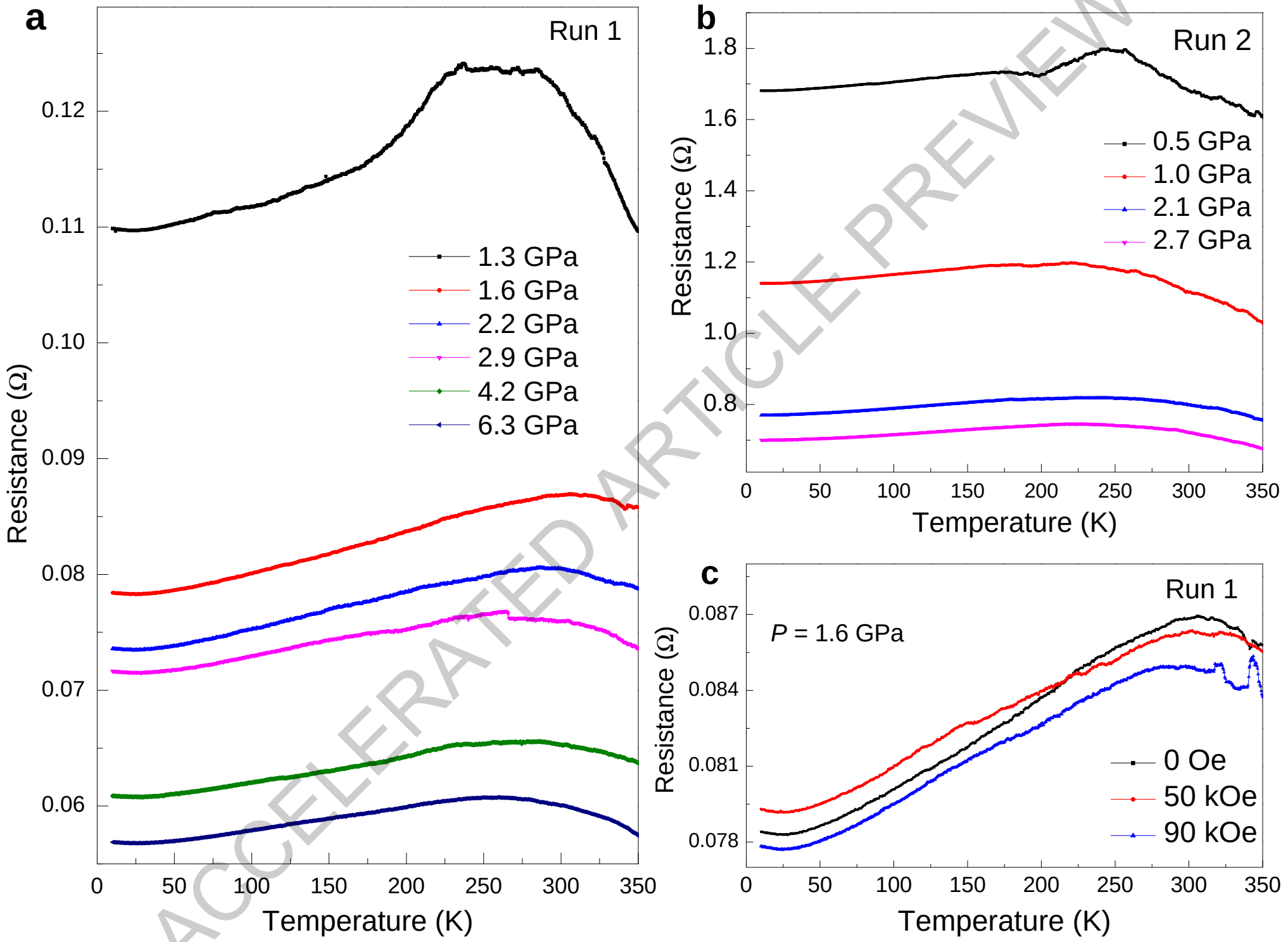

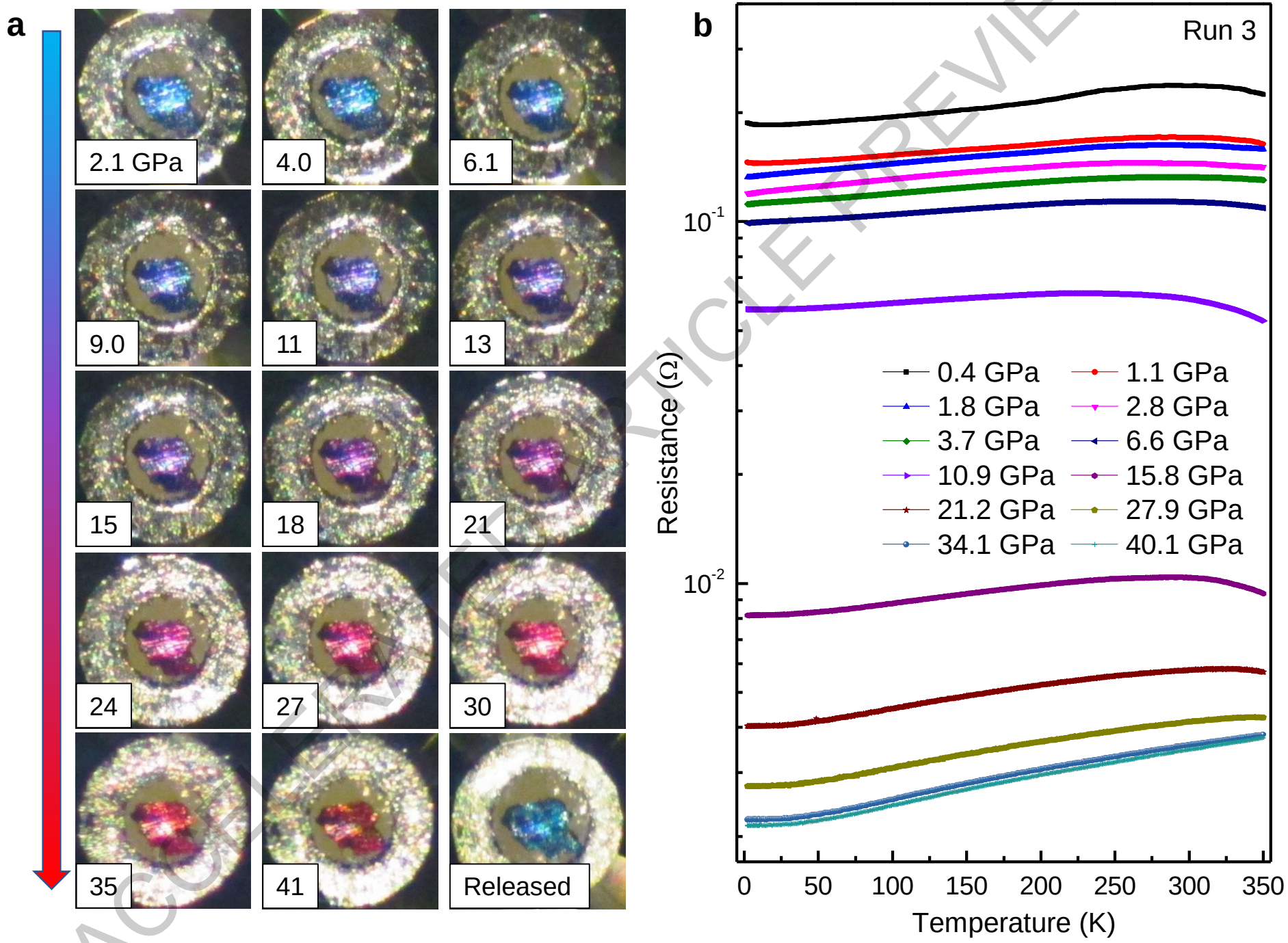

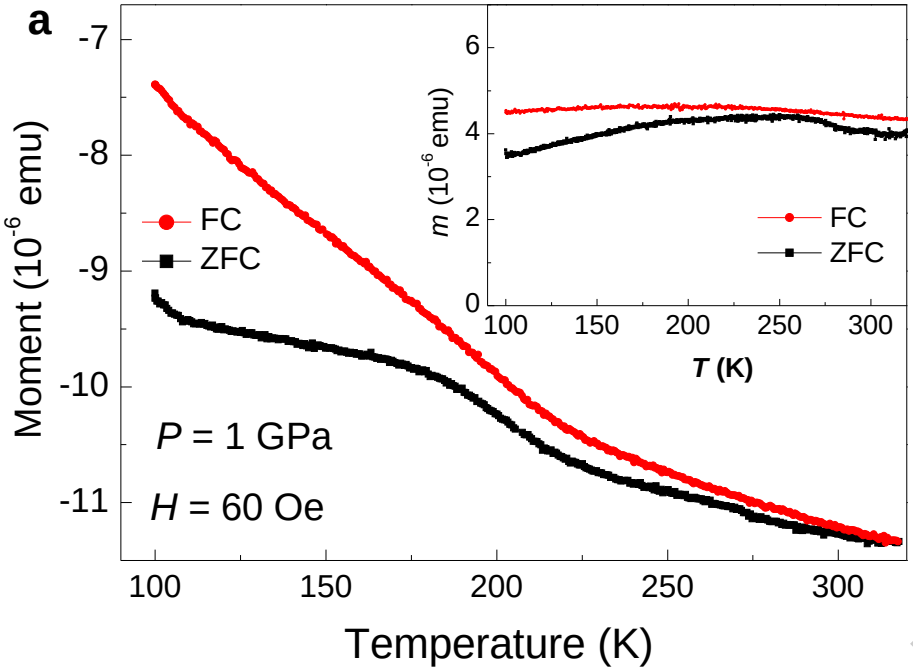

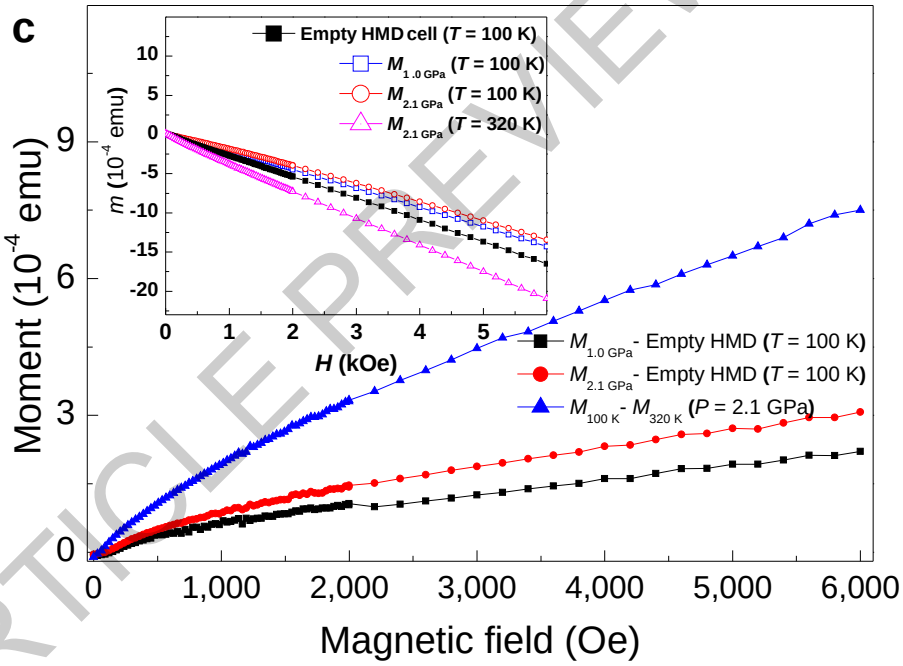

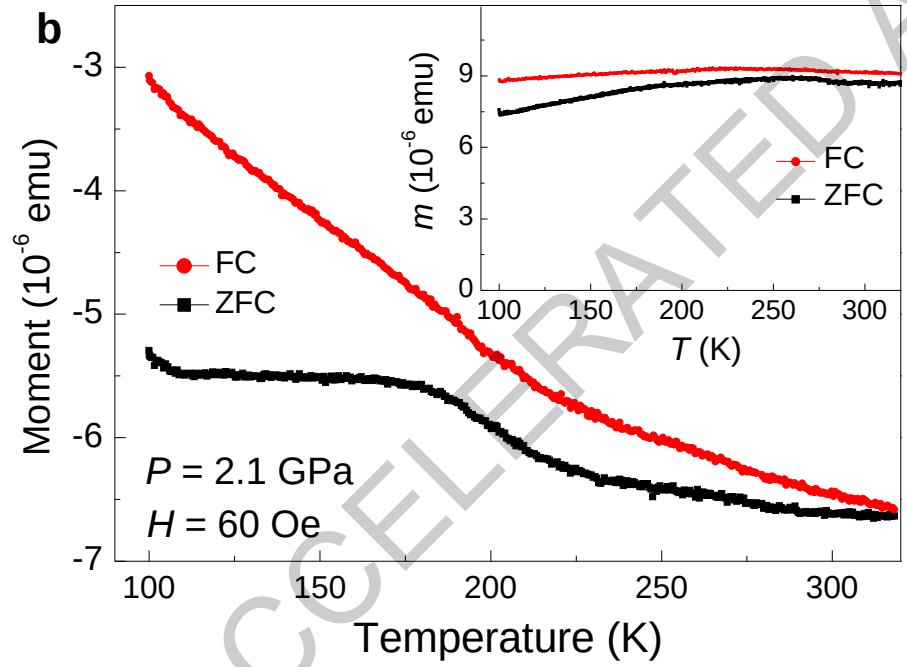

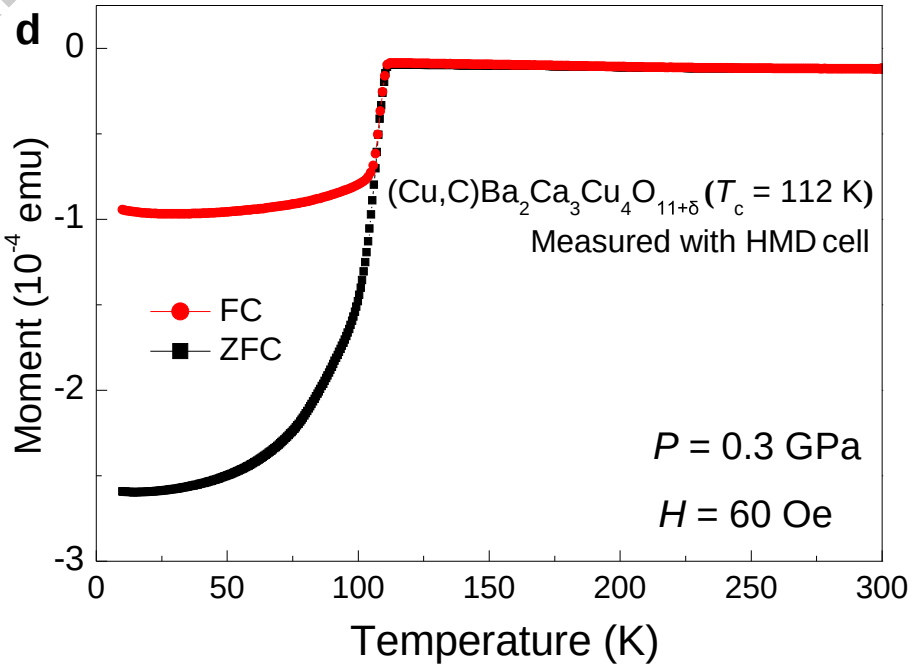

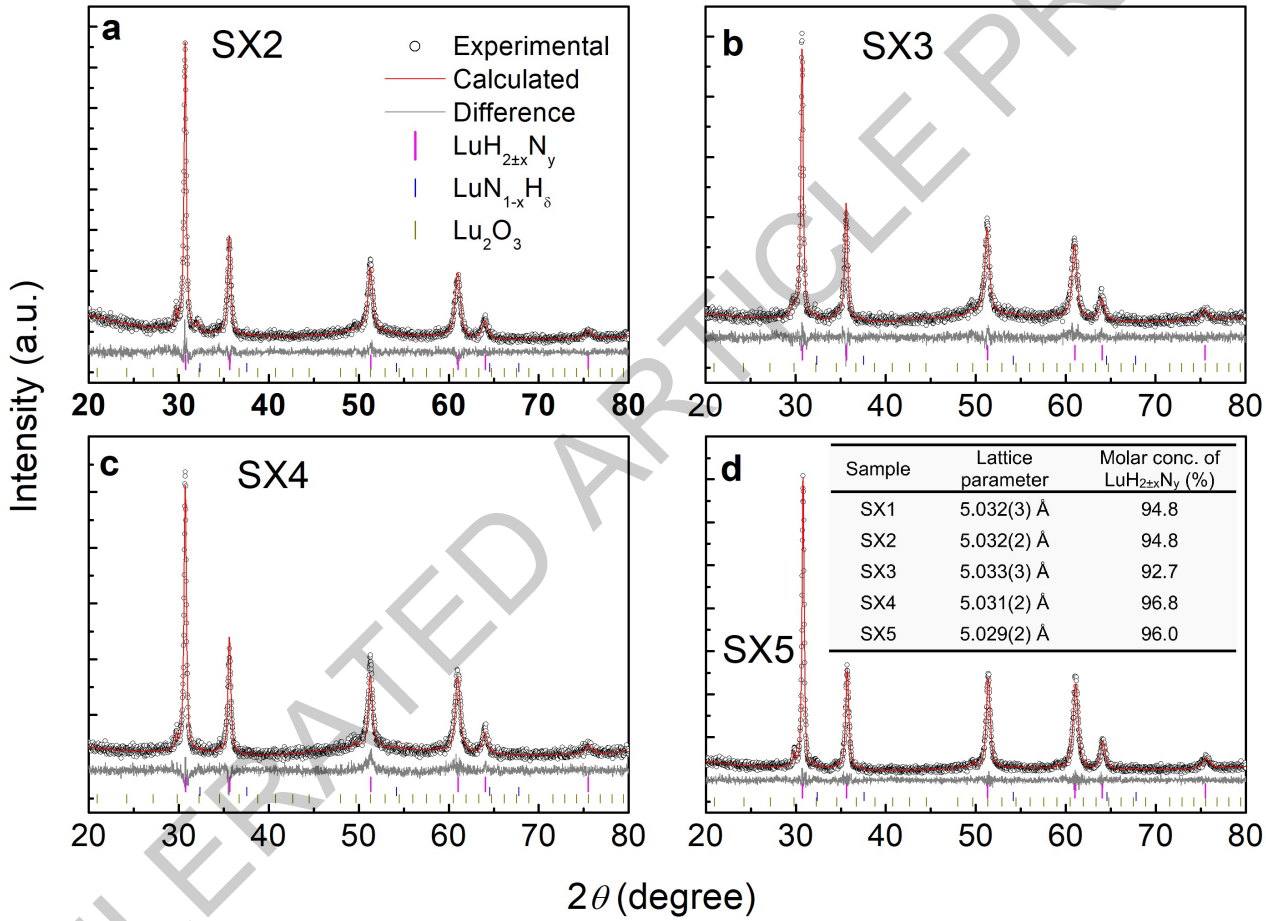

Sample	Lattice parameter	Molar conc. of $LuH_{2\pm x}N_y$ (%)
SX1	5.032(3) Å	94.8
SX2	5.032(2) Å	94.8
SX3	5.033(3) Å	92.7
SX4	5.031(2) Å	96.8
SX5	5.029(2) Å	96.0

Extended Data Fig. 1

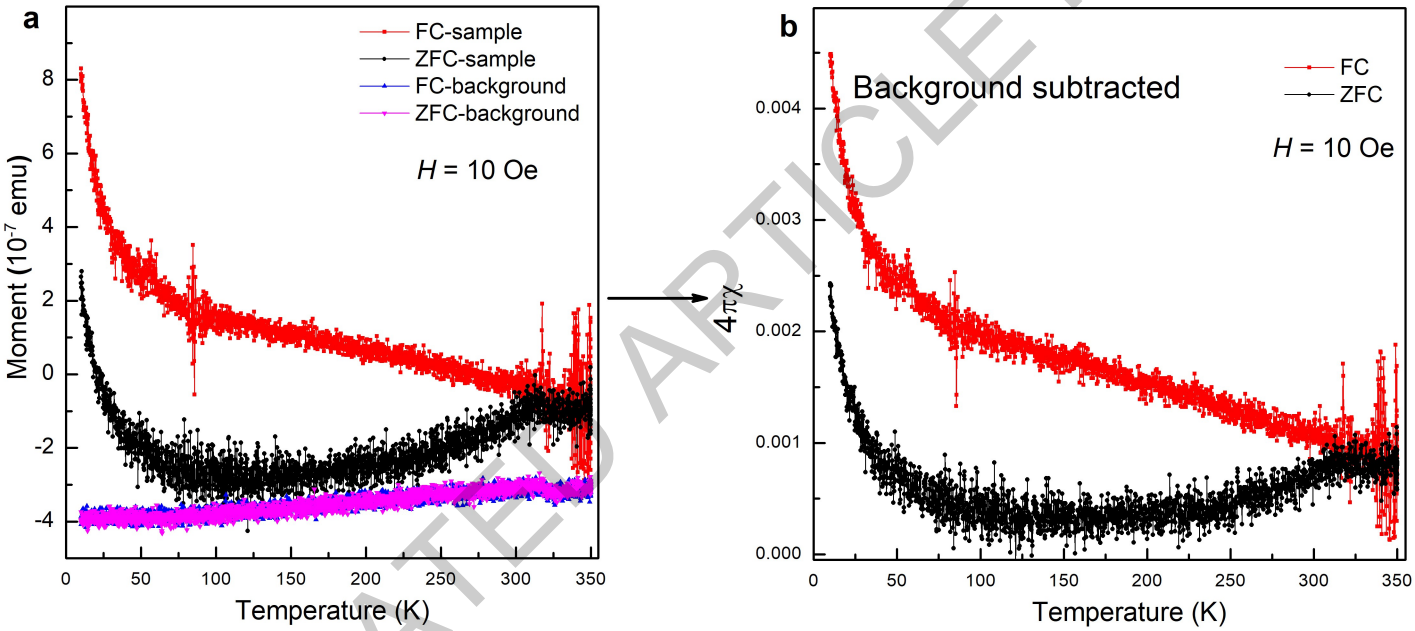

Extended Data Fig. 2

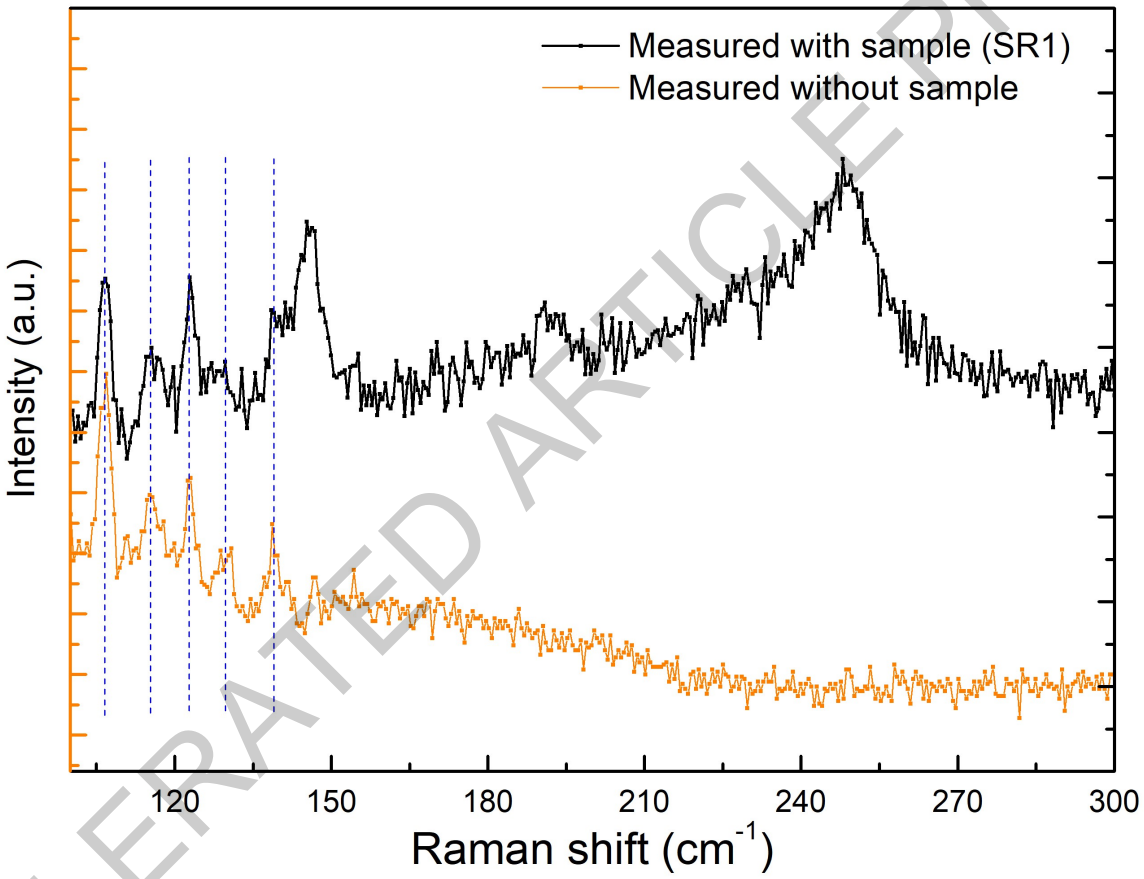

Extended Data Fig. 3

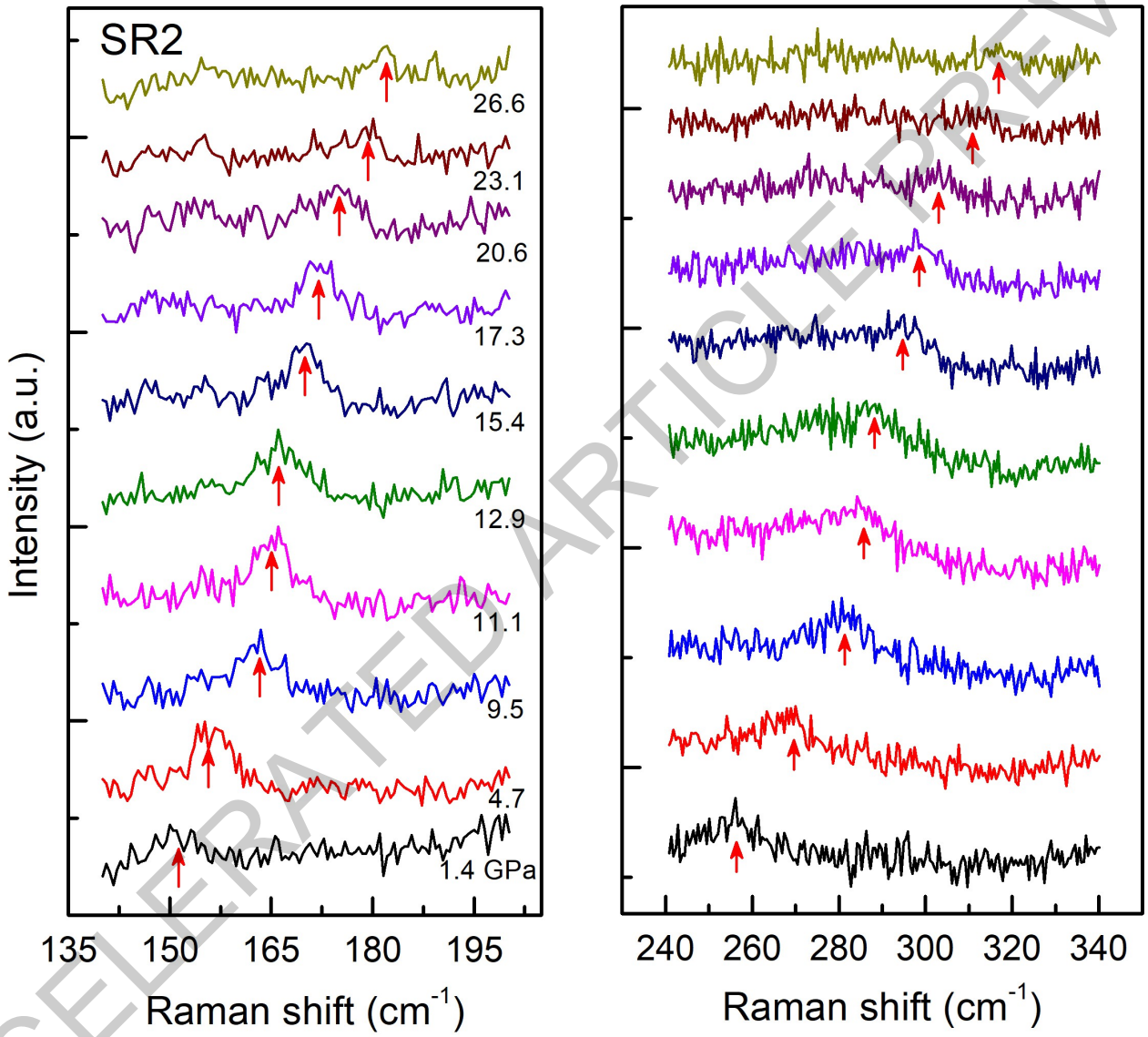

Extended Data Fig. 4

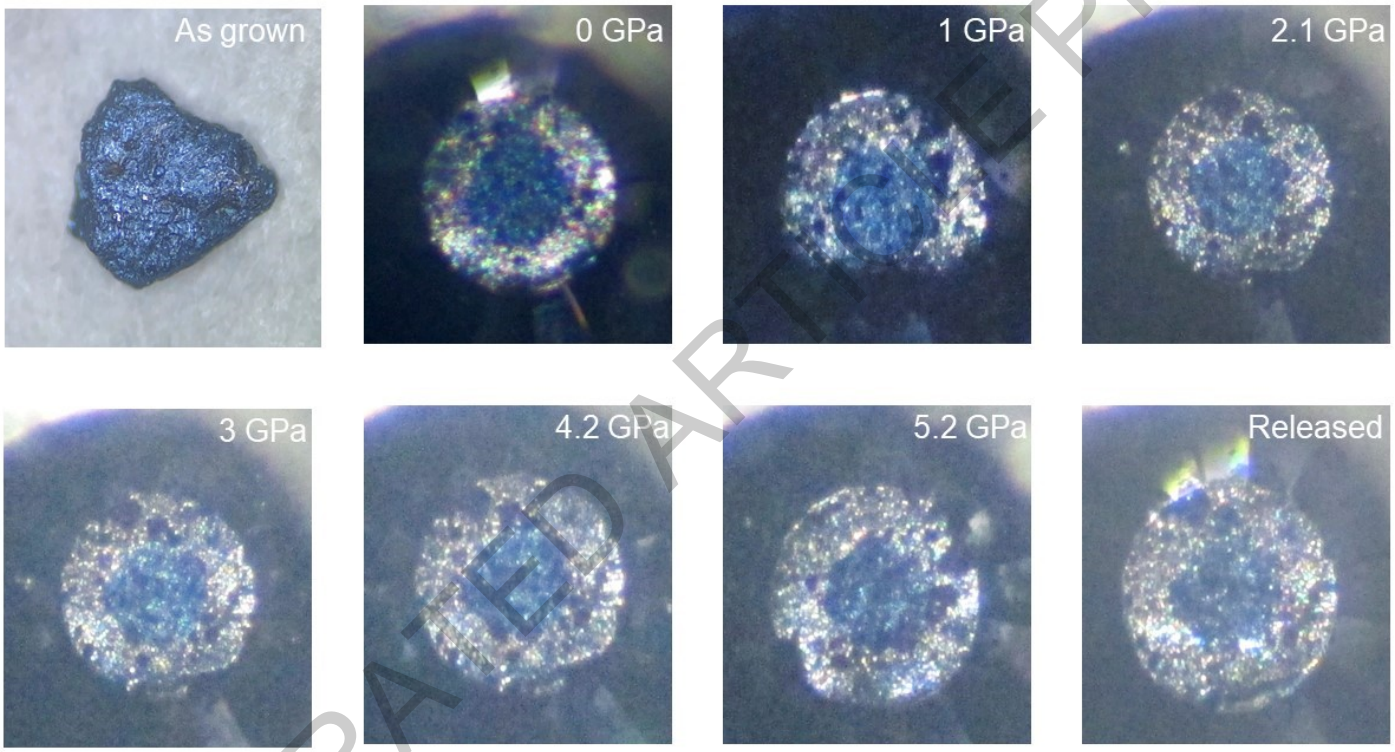

Extended Data Fig. 5

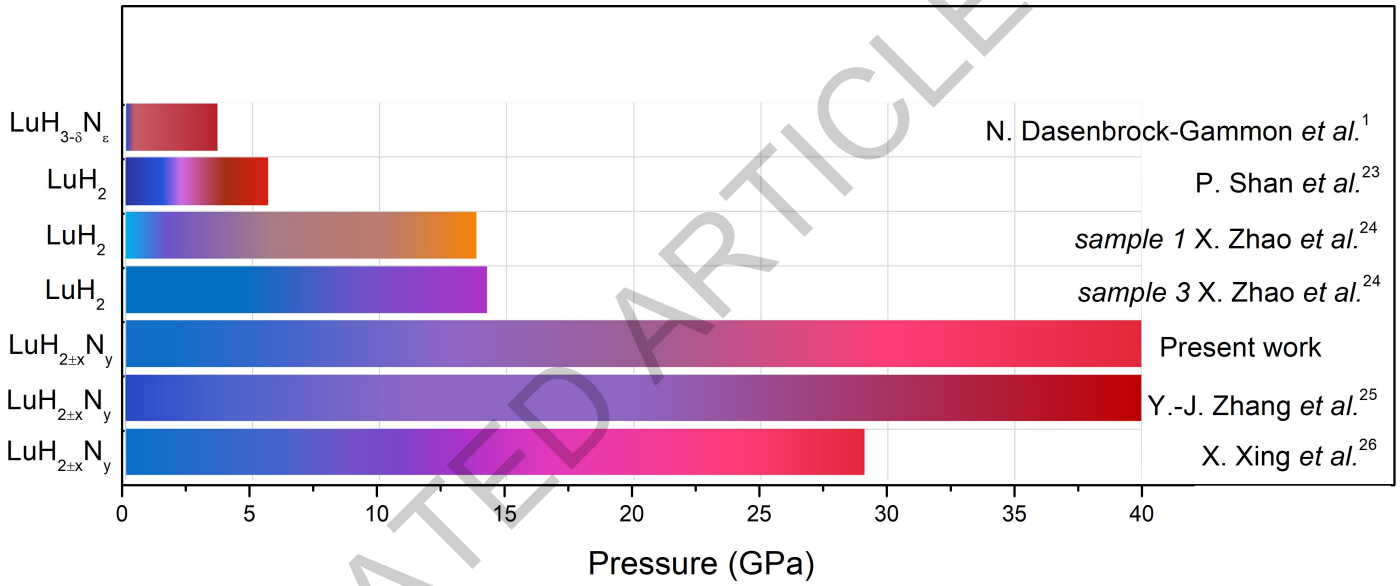

Extended Data Fig. 6

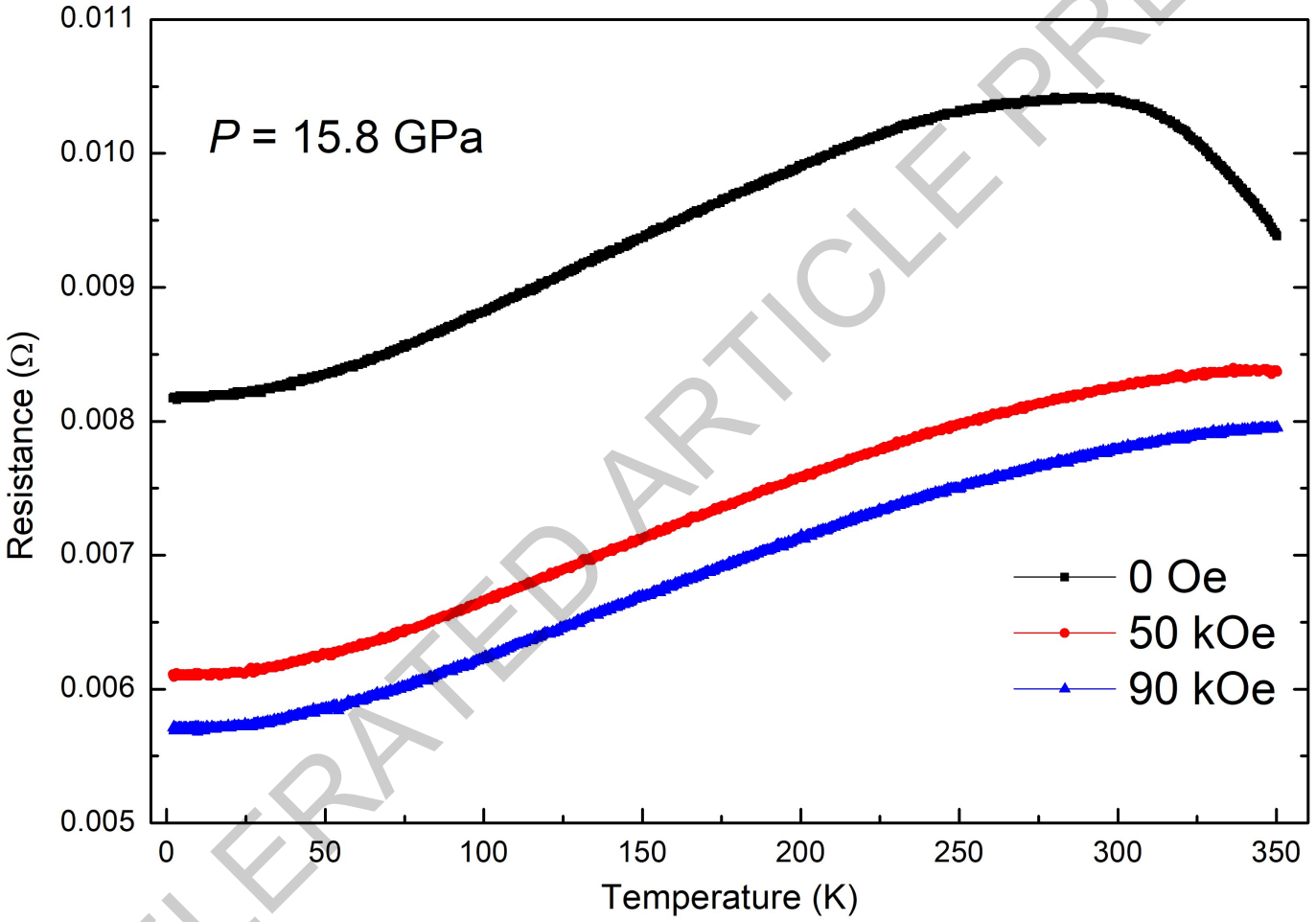

Extended Data Fig. 7

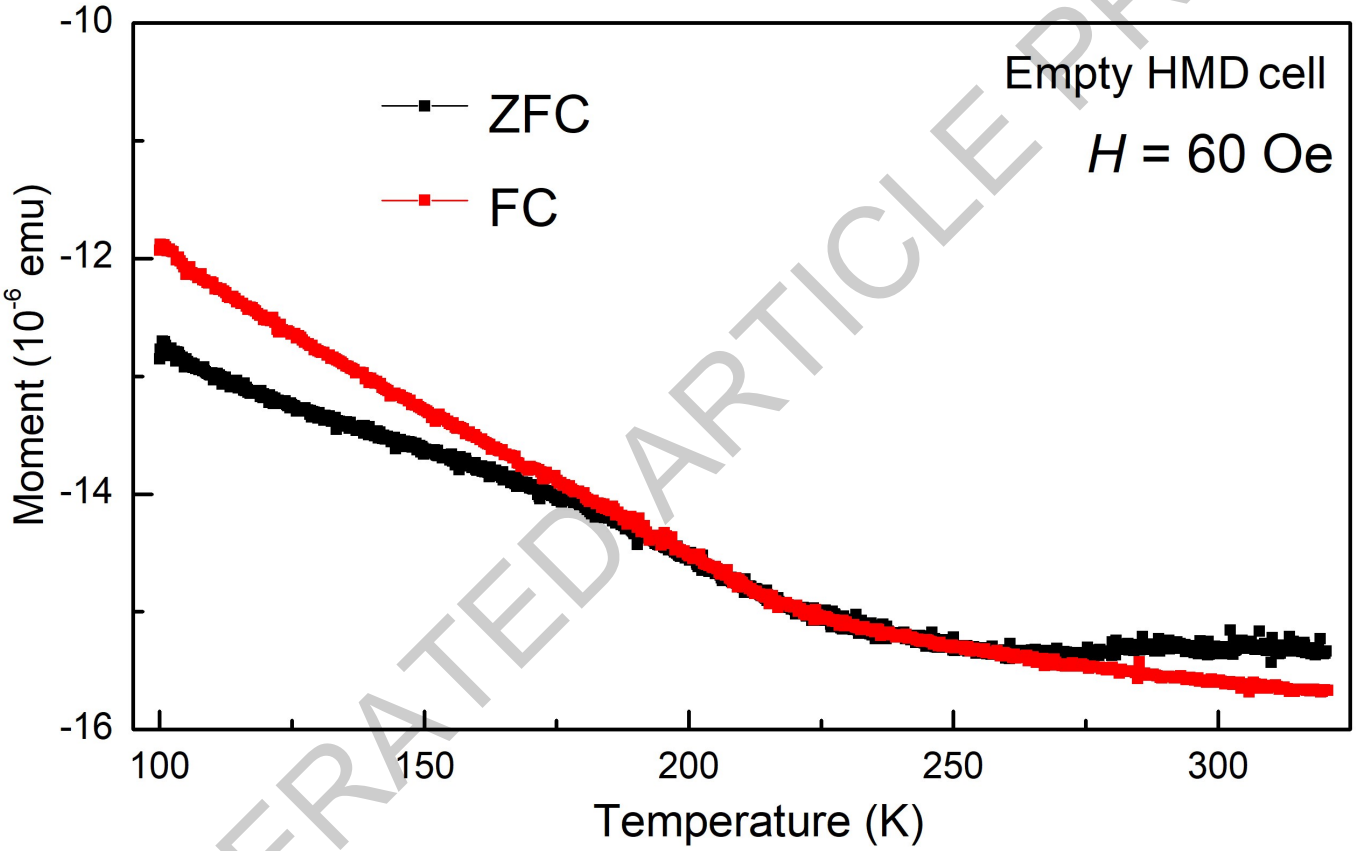

Extended Data Fig. 8

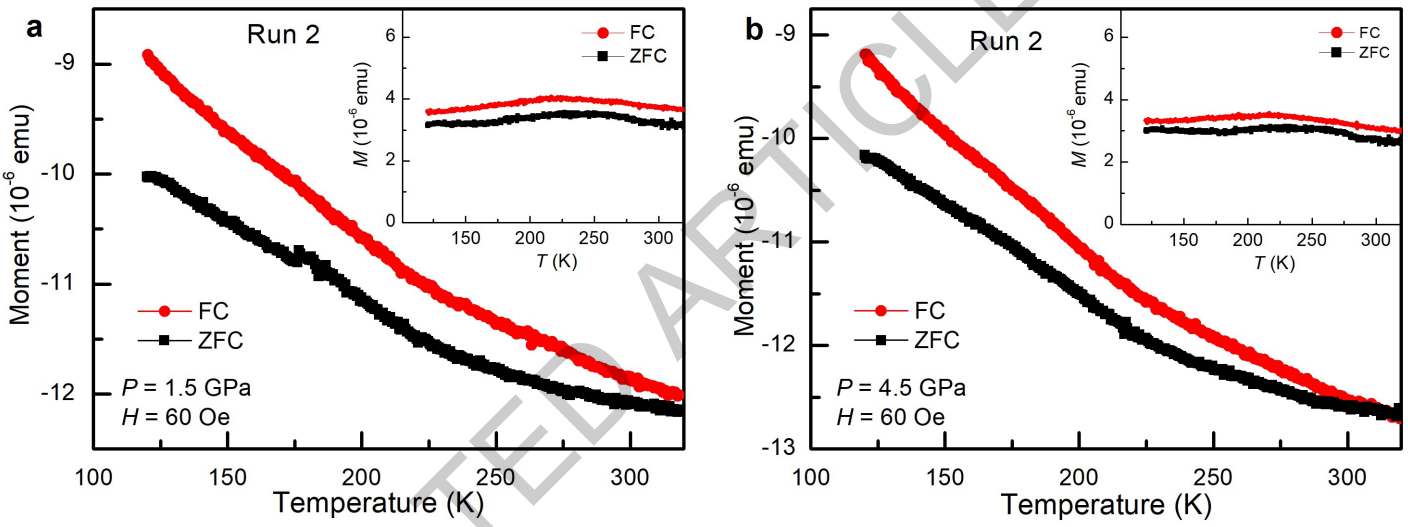

Extended Data Fig. 9

Spot number	Atomic conc. of N (%)
Spot 1	8.26
Spot 4	0.66
Spot 7	1.27
Spot 9	1.78
Other spots	0

Extended Data Table 1